Journal of Materials and Electronic Devices 3 (2024) 13-20

Determination of the Thermodynamic SME Parameters and Related Structure of Arc Melted CuAlNiV HTSMA

Oktay KARADUMAN[1], İskender ÖZKUL[2], Gökhan İSTEK[3], Canan Aksu CANBAY[3*]

[1]Rare Earth Elements Application and Research Center (MUNTEAM), Munzur University, 62000, Tunceli, TÜRKİYE
[2]Department of Mechanical Engineering, Faculty of Engineering, Mersin University, Mersin, TÜRKİYE
[3]Department of Physics, Faculty of Science, Firat University, 23119 Elazig, TÜRKİYE

Low cost Cu-based shape memory alloys (SMAs) have been regarded as potential alternative to the superior NiTi SMAs that are expensive and the most commercial SMAs. Hence, by many researchers have been interested with Cu-based SMAs and studied to develope them and improve their shape memory and other properties. In this work, the quaternary CuAlNiV high-temperature SMA (HTSMA) was manufactured by arc melting technique. Solution treatment for homogenization CuAlNiV alloy and post quenching in iced-brine water were carried out to form the martensite phase (shape memory effect property) in the alloy. Differential calorimetry (DSC and DTA) and X-ray diffraction (XRD) characterization measurements were carried out to detect the thermal and structural shape memory effect properties of the CuAlNiV alloy. The differential scanning calorimetry (DSC) results revealed the powerful reversible martensitic phase transformation peaks in a temperature region above 100 °C, indicating the HTSMA property of the alloy. Many important thermodynamic parameters related to these martensitic transformation reactions of the CuAlNiV HTSMA were determined by making the peak analyses of these transformation peaks. The differential thermal calorimetry (DTA) test result, also showed the martensitic transformation peaks of the alloy, revealed the multiple phase transitions of β'1→ β1($L2_1$)→B2→A2 which occurred consecutively during heating the alloy in the temperature region between room temperature and a high temperature (900 °C). The XRD pattern of the alloy obtained by using CuKα radiation at room temperature revealed the presence of the formed martensite phases in the alloy. All results showed that the fabricated CuAlNiV memory alloy can be utilized as an HTSMA in the relevant SMA applications.

Keywords: *Cu-based shape memory alloy, CuAlNiV HTSMA, Shape memory effect, Arc melting, Martensitic transformation, DSC, DTA*

Submission Date: 23 July 2024
Acceptance Date: 29 August 2024

**Corresponding author: caksu@firat.edu.tr*

1. Introduction

Shape memory alloys (SMAs) [1–3] have been extensively studied mainly due to their unique and magic-like shape memory effect (SME), superelasticity (SE) and good damping properties. These properties made these materials very useful and well reason for utilisation preference in many industry and technology application fields such as actuator, automotive, biomedical, aero-space, robotics, construction, energy harvesting/converting, micro and nano electro-mechanic systems (M/NEMSs), textile, etc.[2–13]. In most of applications nickel-titanium (NiTi) SMAs [14–

17] are preferred to use in applications due to their superior shape memory and superelastic properties. But much cheaper copper-based SMAs, regarded the closest alternative to NiTi SMAs, have still attracted researchers quite well to explore and improve them [18–31].

Polycrystalline Cu-based SMAs have some shortcomings such as brittleness leading to fracture, and thermal instability or instability of martensite and austenite phases that affects transformation temperatures, hysteresis, strain recovery i.e. the shape memory properties [18,26,31–34]. These issues arise mainly from the coarse grains, defects or martensite types and they are also highly dependent on the material production/processing history and the composition of these alloys. A practical recipe frequently used to solve these problems and also to modify the properties of them is doping some grain refining elements such as Be, Ni, Ti, Mn, Fe, Cr, Co, V,Cr Mg etc. in Cu-based SMAs [11,27,35–50]. The shape memory properties of Cu-based SMAs are extremely sensitive to their alloying compositions or their average conduction electron concentration per atom (e/a) ratios which depend on their composition.

Among Cu-based SMAs, CuAlNi alloys have high usage potential in high-temperature shape memory alloy (HTSMA) applications because CuAlNi SMAs exhibit high thermal stability, and good SME and SE properties at temperatures above 100 °C [31]. In this study, the copper-based quaternary CuAlNiV high-temperature shape memory alloy (SMA) with a composition of 69.2Cu-26.6Al-4Ni-0.4V (at%) was produced by arc melting metdod and the effect of minor vanadium addition on the thermal and structural SME properties of CuAlNi alloy was investigated.

2. Experimental

The CuAlNiV high-temperature shape memory alloy with 69.2Cu-26.6Al-4Ni-0.4V (at%) composition was produced by melting the pelletized powder mixture of high purity (%99.9) elements of Cu, Al, Ni, and V in a vacuum arc melter. After arc melting, the obtained as-cast ingot alloy was cut into small test samples and then were homogenized at 900 ºC for 1 hour and immediately quenched in iced-brine water (by this fast cooling, martensite phase was built in the alloy). The differential scanning calorimetry (DSC) tests were carried out by using a Shimadzu 60A label DSC instrument at different 10, 15, 20 and 25 °C/min of heating/cooling rates under an inert argon gas flow of 100 ml/min to examine the presence of a thermally induced shape memory behavior. The differential thermal analysis (DTA) test was taken under same inert gas flow and at a single 25 °C/min of heating/cooling rate between room temperature and 900 °C by using a Shimadzu DTG-60AH instrument for behavior of the alloy at high temperatures. X-ray diffraction (XRD) pattern was obtained at room temperature via a Rigaku Miniflex 600 model X-ray diffractometer (by using CuKα X-rays) to see the peaks indicating presence of the formed martensite phases in the CuAlNiV alloy matrix. EDS (energy dispersive X-ray spectrum) analysis was made to detect the alloying composition of the CuAlNiV alloy by using a SEM-Hitachi SU3500 instrument at room temperature.

3. Results and Discussion

The DSC curves of the fabricated CuAlNiV alloy (presented in Fig.1) show the down endothermic and up exothermic solid-to-solid reaction peaks indicating the reversible martensitic phase transformation peaks of the CuAlNiV alloy [26,51,52]. Since these peaks occurred (or the start and finish temperatures of these martensitic transformation peaks fall) in a temperature range above 100 °C, the produced CuAlNiV alloy is labelled as a high-temperature shape memory alloy [4,26]. The zig-zags seen formed on the peaks at 10 and 15 °C/min of rates are caused by the transformation of the multiple micro-nano interfaces. The decrease in stored elastic energy during the direct transformation at 10 °C/min of rate causes a increment in the A_s temperature during the reverse transformation at 15 °C/min of rate [31].

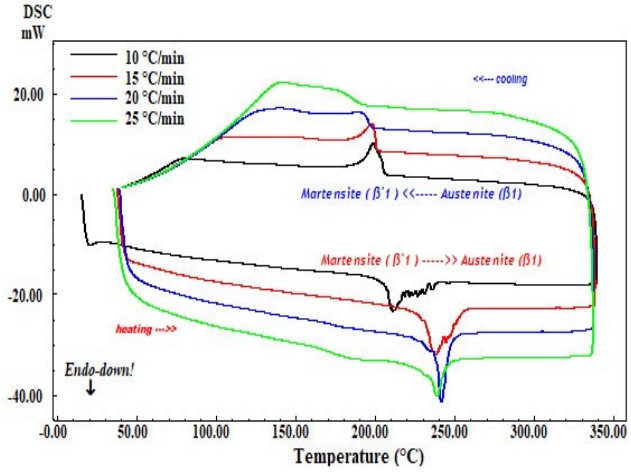

Fig.1. The sequentially cycling DSC heating/cooling curves taken at different 10, 15, 20 and 25 °C/min of heating/cooling rates show the reverse martensite to austenite (M→A) transformation on heating fragments of these curves and the corresponding forward austenite to martensite (A→M) transformation on cooling fragments of these curves.

The characteristic martensitic transformation temperatures , the peak start, finish and max temperatures (A_s, A_f, A_{max}, M_s, M_f) of the fabricated CuAlNiV HTSMA which directly determined from DSC tangent peak analyses data at each heating/cooling rate are presented in Table 1. Accordingly,

it is seen that the transformation temperatures are in the range (the lowest M_f and the highest A_f) of 171.31 °C and 251.90 °C, and the average range extends from 183.57 °C upto 240.83 °C. Some other corresponding transformational thermodynamic parameters values obtained directly by these peak analyses and by calculations were listed in Table 1, too. One example of these peak analyses that was made on the DSC curve taken at 20 °C/min of heating/cooling rate is given in Fig.2. As seen from Table 1 and Fig.2, the transformation temperatures at 20 °C/min of heating/cooling is in the range from 171.31 °C upto 247.03 °C. A transformation temperatures range from 90 °C (M_f) upto 179 °C (A_f) obtained at 20 °C/min of heating/cooling rate was reported in a previous work [53] made on an another CuAlNiV alloy with a compositon of 68.9Cu-27.1Al-3.6Ni-0.4V (at%). Although the same amount (0.4 at%) of vanadium was used in our work here, the use of 0.4 at% higher nickel together with 0.5 at% lower aluminium in our work resulted in higher transformation temperatures, so 81 °C higher M_f and 68 °C higher A_f.

Table-1: The characteristic martensitic transformation temperatures and thermodynamic parameters of the of CuAlNiV HTSMA obtained from the DSC peak analyses data.

Heating/cooling rate (°C/min)	A_s (°C)	A_f (°C)	A_{max} (°C)	M_s (°C)	M_f (°C)	A_s-M_f (°C)	T_0 (°C)	$\Delta H_{M\rightarrow A}$ (J/g)	$\Delta S_{M\rightarrow A}$ (J/g°C)
10	207.21	219.56	211.25	206.01	192.60	14.61	212.79	14.92	0.0701
15	231.45	251.90	238.41	201.43	188.41	43.04	226.67	13.75	0.0607
20	238.21	247.03	241.93	198.08	171.31	66.90	222.56	7.68	0.0345
25	233.01	244.82	238.93	199.25	181.94	51.07	222.04	4.58	0.0206
Avg.	227.47	240.83	232.63	201.19	183.57	43.91	221.01	10.23	0.0465

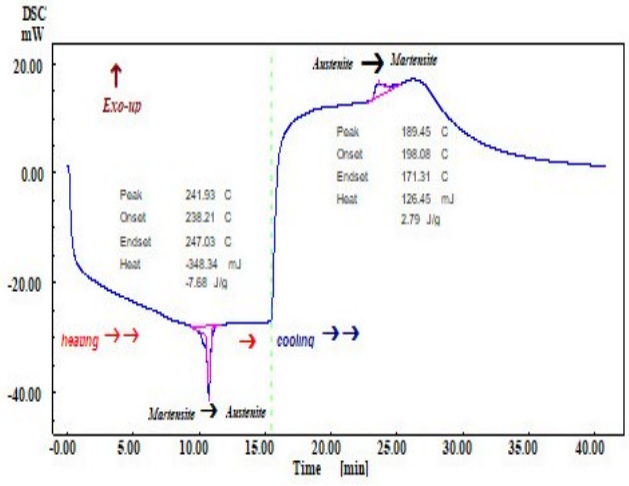

Fig.2. The forward and reverse martensitic transformation peaks on the DSC curve on x-time-axis taken at 20 °C/min of heating/cooling rate analyzed by tangent method by using DSC software. The two analysis data sets of these peaks include peak start (onset), finish (endset), maximum (peak) temperatures and enthalpy (J/g) change values.

The values of the thermal equilibrium temperature (T_0), at where there is no difference between the Gibbs (chemical) free energies of martensite and austenine phases, were also given in Table 1. The values of T_0 at each heating/cooling rate were determined by using formula [11] below;

$$T_o = \frac{1}{2}(A_f + M_s) \quad (1)$$

The amounts of the entropy change, ΔS (also given in Table 1) occurred during M→A transformations, as another transformational thermodynamic parameter, were determined by using the enthalpy ΔH change values in the formula [11,26] given as below;

$$\Delta S_{M\rightarrow A} = \frac{\Delta H_{M\rightarrow A}}{T_o} \quad (2)$$

The kinetic activation energy (E_a) parameter is a determining factor in occurance of martensitic phase transitions and crystallization behavior of the alloy. Martensitic transformations are first-order reactions. Therefore, the given-below formula from Kissinger [54] was suitably used to calculate the E_a value of the alloy;

$$\frac{d\left[ln\left(\frac{\phi}{T_m^2}\right)\right]}{d\left(\frac{1}{T_m}\right)} = -\frac{E_a}{R} \quad (3)$$

where; ϕ stands for the heating/cooling rate, T_m is the transformation maximum peak temperature (A_{max}) and R is the universal gas constant (R=8.314 J/mol.K). The left fraction term of Eq.3 represents the change of activation energy. The value of this fraction is found as the linear fitting slope value of $ln(\Phi/T_m^2)$ vs. $1000/T_m$ plot which is presented in Fig.3. By substituting this slope value in Eq.3, the E_a value of the reverse martensitic phase transition of the fabricated CuAlNiV HTSMA was found as 40.52 kJ/mol.

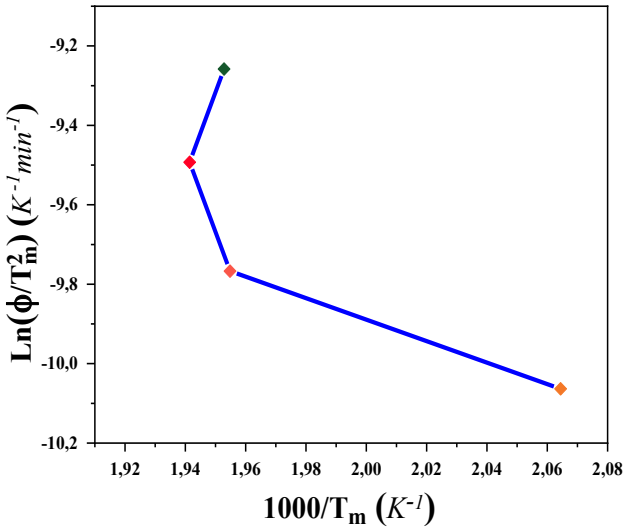

Fig.3. The activation energy change plot of the reverse martensitic transformation of the CuAlNiV HTSMA.

The DTA curve, given in Fig.4, shows the other thermally induced reactions in the CuAlNiV HTSMA at high temperatures and also shows the reversible martensitic tansformation peaks. When starting to look from the far right to the far left on the down heating segment of this DTA curve, some peaks of thermal events formed as the responsive behavior of the alloy indicate the phase transition chain that follows as: martensite (β1′) →austenite (β1, $L2_1$) → B2 (metastable cubic) → precipitating → eutectoid recomposition → B2 (ordered cubic) →A2 (disordered cubic). This phase transition chain is commonly seen thermal behavior of Cu-based SMAs [26,55–58].

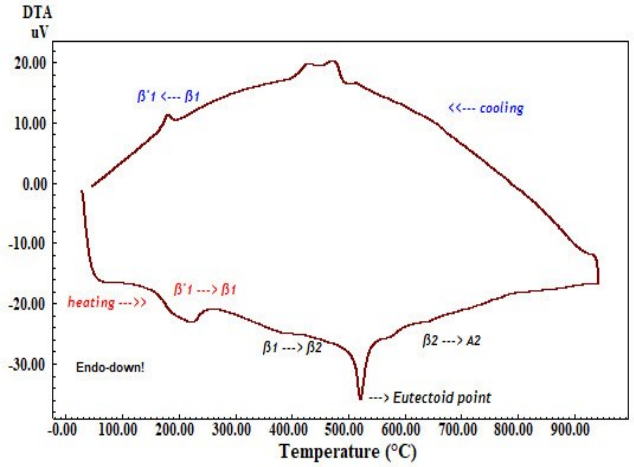

Fig.4. The cycling DTA heating/cooling curve of the CuAlNiV HTSMA taken at single 25 °C/min of heating/cooling rate.

The detected EDS atomic (at%) composition of 69.2Cu-26.6Al-4Ni-0.4V (at%) shows the fractions of the alloying elements' atoms in the CuAlNiV HTSMA. Average electron concentration per atom ratio (e/a ratio) of the CuAlNiV alloy was found as 1.56 by using the atomic (at%) fractions of the alloying elements in the formula [26] given as below;

$$\frac{e}{a} = f_{Cu}v_{Cu} + f_{Al}v_{Al} + f_{Ni}v_{Ni} + f_{V}v_{V} \quad (4)$$

where; f is the atomic fractions of the alloying elements, and v refers to the valence electron values of these alloying elements (here; v_{Cu} =1, v_{Al}=3, v_{Ni}=2 and v_{V}=2). The e/a ratio of the CuAlNiV is found above the e/a ratio range of 1.45-1.51 which range is regarded as a theoretical condition for Cu-based alloys to have most probably a shape memory effect [1,26]. Also, in this e/a ratio range Cu-based SMAs have two different martensite forms (β1′ and γ1′) together. Above this range (for e/a ratios higher than 1.51) the γ1′ martensite phase is expected to form dominantly over the β1′ martensite in the alloy, and vice-versa [26]. To see this structural expectation the XRD result of the CuAlNiV HTSMA is given in Fig.5.

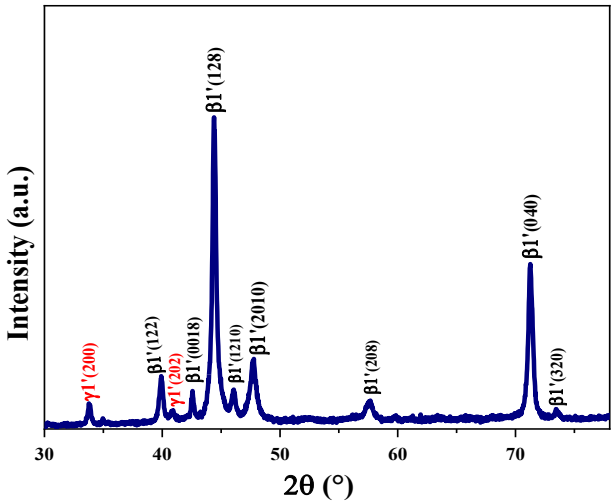

Fig.5. The XRD pattern of the CuAlNiV HTSMA.

The XRD pattern of the CuAlNiV HTSMA shows presence of the formed martensitic phases in the alloy at room temperature. The main peak is β1′ (128) martensite peak, and the others are also some β1′ and γ1′ type martensite peaks [26,42,52,53,55,59,60]. The XRD pattern of the CuAlNiV HTSMA shows the co-existence of monoclinic β1′ (18R) and orthorhombic γ1′ (2H) type martensite phases just as predicted by the e/a ratio of the alloy. As seen on the XRD pattern of the alloy, the β1′ peaks are the main or dominant martensite peaks. According to the e/a value of the CuAlNiV alloy, the γ1′ peaks were normally expected to be the dominant over β1′ and expected to be observed more intense and no fewer than the β1′ peaks. What caused that γ1′ peaks are observed fewer and weaker than some of the higher β1′ peaks is originated from that the hexagonal 2H (γ1′) phase has less symmetry (or more amorphism) than the monoclinical β1′ does [12]. Because, the X-rays scattering domain (spherical or ellipsoidal particle) size of β1′

martensite or the number of coherently scattered X-rays from β1′ martensite is larger than that of γ1′ martensite (while a plane of hexagonal γ1′ unit cell made of three monoclinic-like cells scatters one X-ray, a plane of monoclinical β1′ unit cell scatters three X-ray and also absorbes less) [12].

The crystallite size of the alloy was also calculated by using the well-known Debye-Scherrer formula [26,61] given as below;

$$D = \frac{0.9\lambda}{B_{\frac{1}{2}} \cos\theta} \quad (5)$$

where; λ is the wavelength of the X-ray (CuKα radiation, λ= 0.15406 nm), $B_{1/2}$ is the full width at half maximum (FWHM) value of the highest (main) peak, and θ is the Bragg angle of X-ray diffraction. The mean size of the ordered (crystalline) domains, i.e. the Debye-Scherrer crystallite size (D) of the CuAlNiV HTSMA was found as 28.34 nm by using the FWHM value (0.3029) of the main β1′ (128) peak at the 2θ angle of 44.37°.

4. Conclusions

The quaternary Cu-Al-Ni-V HTSMA was produced succesfully by arc melting and the shape memory effect characterization of the alloy was made by differential calorimetry (DSC, DTA) and structural (XRD, EDS) measurements. The DSC and DTA results showed the powerful reversible martensitic transformation peaks at the temperatures above 100 °C and ranging approximately at between 171 °C (M_f) and 251 °C (A_f). It was understood that by use of 0.4 at% of more nickel resulted in higher transformation temperatures; at least 81 °C higher M_f and 68 °C higher A_f. The heating segment of DTA curve showed the multiple phase transitions chain peaks of β1′(or β1′+γ1′) → β1($L2_1$) → B2 → A2 phase transitions which is commonly seen thermal behavior of the Cu-based shape memory alloys. The XRD result showed the co-existence of β1′and γ1′ type martensites which constitute the crystallographic base mechanism for the shape memory effect property of the fabricated CuAlNiV HTSMA. The findings obtained by thermokinetic shape memory effect analysis of the CuAlNiV HTSMA and the alloy itself can be useful in HTSMA and related applications.

Acknowledgments:

This research work is a part of thesis works of Gökhan İSTEK mastering in general physics in Physics Department, Science Faculty, Firat University.

References:

[1] Otsuka K, Wayman CM. Shape memory materials. Cambridge University Press; 1999.

[2] Concilio A, Antonucci V, Auricchio F, Lecce L, Sacco E (Eds.). Shape Memory Alloy Engineering. 2nd ed. Elsevier; 2021. https://doi.org/10.1016/C2018-0-02430-5.

[3] Rao A, Srinivasa AR, Reddy JN. Introduction to shape memory alloys. SpringerBriefs in Applied Sciences and Technology 2015:1–31. https://doi.org/10.1007/978-3-319-03188-0_1.

[4] López-Ferreño I, Gómez-Cortés JF, Breczewski T, Ruiz-Larrea I, Nó ML, San Juan JM. High-temperature shape memory alloys based on the Cu-Al-Ni system: design and thermomechanical characterization. Journal of Materials Research and Technology 2020;9. https://doi.org/10.1016/j.jmrt.2020.07.002.

[5] Fernandes DJ, Peres R V., Mendes AM, Elias CN. Understanding the Shape-Memory Alloys Used in Orthodontics. ISRN Dent 2011;2011:1–6. https://doi.org/10.5402/2011/132408.

[6] Riccio A, Sellitto A, Ameduri S, Concilio A, Arena M. Shape memory alloys (SMA) for automotive applications and challenges. Shape Memory Alloy Engineering: For Aerospace, Structural, and Biomedical Applications 2021:785–808. https://doi.org/10.1016/B978-0-12-819264-1.00024-8.

[7] Ma J, Karaman I, Noebe RD. High temperature shape memory alloys. International Materials Reviews 2010;55:257–315. https://doi.org/10.1179/095066010X12646898728363.

[8] Hartl DJ, Lagoudas DC. Aerospace applications of shape memory alloys. Proceedings of the Institution of Mechanical Engineers, Part G: Journal of Aerospace Engineering 2007;221:535–52. https://doi.org/10.1243/09544100JAERO211.

[9] Fu YQ, Luo JK, Flewitt AJ, Huang WM, Zhang S, Du HJ, et al. Thin film shape memory alloys and microactuators. Int J Computational Materials Science and Surface Engineering 2009;2:208–26. https://doi.org/10.1504/IJCMSSE.2009.027483.

[10] Fu YQ, Luo JK, Huang WM, Flewitt AJ, Milne WI. Thin film shape memory alloys for optical sensing applications. J Phys Conf Ser 2007;76. https://doi.org/10.1088/1742-6596/76/1/012032.

[11] Karaduman O, Canbay CA, Dere A, Orman Y, Al-Ghamdi AA, Al-Sehemi AG, et al. Smart alloy metalized novel photonic NEMS photodiode with CuAlV/n-Si/Al junction structure. Phys Scr 2024;99. https://doi.org/10.1088/1402-4896/ad2047.

[12] Canbay CA, Karaduman O. The photo response properties of shape memory alloy thin film based

photodiode. J Mol Struct 2021;1235:130263. https://doi.org/10.1016/J.MOLSTRUC.2021.130263.

[13] Muthukumarana S, Messerschmidt MA. Clothtiles: A prototyping platform to fabricate customized actuators on clothing using 3d printing and shape-memory alloys. Conference on Human Factors in Computing Systems - Proceedings 2021. https://doi.org/10.1145/3411764.3445613.

[14] Kim WC, Lim KR, Kim WT, Park ES, Kim DH. Recent advances in multicomponent NiTi-based shape memory alloy using metallic glass as a precursor. Prog Mater Sci 2021;118. https://doi.org/10.1016/j.pmatsci.2020.100756.

[15] Mwangi JW, Nguyen LT, Bui VD, Berger T, Zeidler H, Schubert A. Nitinol manufacturing and micromachining: A review of processes and their suitability in processing medical-grade nitinol. J Manuf Process 2019;38:355–69. https://doi.org/https://doi.org/10.1016/j.jmapro.2019.01.003.

[16] Kauffman GB. The Story of Nitinol: The Serendipitous Discovery of the Memory Metal and Its Applications. The Chemical Educator 1997;2:1–21. https://doi.org/10.1007/s00897970111a.

[17] Nespoli A, Passaretti F, Szentmiklósi L, Maróti B, Placidi E, Cassetta M, et al. Biomedical NiTi and β-Ti Alloys: From Composition, Microstructure and Thermo-Mechanics to Application. Metals (Basel) 2022;12:406. https://doi.org/10.3390/met12030406.

[18] Mazzer EM, Da Silva MR, Gargarella P. Revisiting Cu-based shape memory alloys: Recent developments and new perspectives. J Mater Res 2022;37:162–82. https://doi.org/10.1557/s43578-021-00444-7.

[19] Ashwath J, Pavithran M, Santosh S. Fabrication, processing and characterization of Cu-based smart alloys. Mater Today Proc 2023;72:2497–500. https://doi.org/10.1016/j.matpr.2022.09.528.

[20] Najah Saud Al-Humairi S. Cu-Based Shape Memory Alloys: Modified Structures and Their Related Properties. Recent Advancements in the Metallurgical Engineering and Electrodeposition, IntechOpen; 2020, p. 25. https://doi.org/10.5772/intechopen.86193.

[21] Sampath V, Gayathri SV, Srinithi R. Experimental and theoretical analyses of transformation temperatures of Cu-based shape memory alloys. Bulletin of Materials Science 2019;42. https://doi.org/10.1007/s12034-019-1911-4.

[22] Gómez-Cortés JF, Fuster V, Pérez-Cerrato M, Lorenzo P, Ruiz-Larrea I, Breczewski T, et al. Superelastic damping at nanoscale in ternary and quaternary Cu-based shape memory alloys. J Alloys Compd 2021;883:160865. https://doi.org/10.1016/j.jallcom.2021.160865.

[23] Dasgupta R. A look into Cu-based shape memory alloys: Present scenario and future prospects. J Mater Res 2014;29:1681–98. https://doi.org/10.1557/jmr.2014.189.

[24] Tian J, Zhu W, Wei Q, Wen S, Li S, Song B, et al. Process optimization, microstructures and mechanical properties of a Cu-based shape memory alloy fabricated by selective laser melting. J Alloys Compd 2019;785:754–64. https://doi.org/10.1016/j.jallcom.2019.01.153.

[25] Alaneme KK, Anaele JU, Okotete EA. Martensite aging phenomena in Cu-based alloys: Effects on structural transformation, mechanical and shape memory properties: A critical review. Sci Afr 2021;12:e00760. https://doi.org/10.1016/j.sciaf.2021.e00760.

[26] Canbay CA, Karaduman O, Ünlü N, Baiz SA, Özkul İ. Heat treatment and quenching media effects on the thermodynamical, thermoelastical and structural characteristics of a new Cu-based quaternary shape memory alloy. Compos B Eng 2019;174:106940. https://doi.org/10.1016/j.compositesb.2019.106940.

[27] de Souza JS, de Oliveira MCL, Antunes RA, da Silva RAG. Quaternary CuAlMn-based alloys with Gd and Sn additions: Surface chemistry and corrosion behavior in sodium chloride solution. Journal of Materials Research and Technology 2022;16:1213–30. https://doi.org/10.1016/j.jmrt.2021.12.064.

[28] Ferreira RO, Silva LS, Silva RAG. Thermal behavior of as-annealed CuAlMnAgZr alloys. J Therm Anal Calorim 2021;146:595–600. https://doi.org/10.1007/s10973-020-10002-8.

[29] Karaduman O, Özkul İ, Canbay CA. Kinetic and structural study on CuAlMnNi shape memory alloy with a novel composition. Advanced Engineering Science 2021;1:13–9.

[30] Özkul İ, Karaduman O, Canbay CA. Effects of Ga, Nb, V, Zr, and Cr on the crystal structures and thermal behavior of CuAlMn shape memory alloys. Proc Inst Mech Eng C J Mech Eng Sci 2023. https://doi.org/10.1177/09544062231193795.

[31] Silva ÍJA, Silva DDS, Lima BASG, Feitosa FRP, Brito ICA, Caluête RE, et al. Study of the thermodynamic parameters, microstructure and mechanical properties of a CuAlNi shape memory alloy produced with recycled aluminum. Mater Today Commun 2023;36:106527. https://doi.org/10.1016/j.mtcomm.2023.106527.

[32] Sutou Y, Kainuma R, Ishida K. Effect of alloying elements on the shape memory properties of ductile Cu–Al–Mn alloys. Materials Science and

Engineering: A 1999;273–275:375–9. https://doi.org/10.1016/S0921-5093(99)00301-9.

[33] Canbay C, Karaduman O, Ibrahim PA, Ozkul I. Thermostructural shape memory effect observations of ductile Cu-Al-Mn smart alloy. Advances in Materials Research 2021;10:45–56. https://doi.org/https://doi.org/10.12989/amr.2021.10.1.045.

[34] Pushin VG, Kuranova NN, Svirid AE, Uksusnikov AN, Ustyugov YM. Design and Development of High-Strength and Ductile Ternary and Multicomponent Eutectoid Cu-Based Shape Memory Alloys: Problems and Perspectives. Metals (Basel) 2022;12. https://doi.org/10.3390/met12081289.

[35] Yang J, Wang QZ, Yin FX, Cui CX, Ji PG, Li B. Effects of grain refinement on the structure and properties of a CuAlMn shape memory alloy. Materials Science and Engineering A 2016;664:215–20. https://doi.org/10.1016/j.msea.2016.04.009.

[36] Yao C, Yin F, Ji P, Hao G, Jiao Z, Liu L, et al. Effects of grain refinement on the microstructures and damping behaviors of a Cu–Al–Ni–Mn–Ti shape memory alloy. Intermetallics (Barking) 2021;138:107315. https://doi.org/10.1016/j.intermet.2021.107315.

[37] Sutou Y, Omori T, Yamauchi K, Ono N, Kainuma R, Ishida K. Effect of grain size and texture on pseudoelasticity in Cu-Al-Mn-based shape memory wire. Acta Mater 2005;53:4121–33. https://doi.org/10.1016/j.actamat.2005.05.013.

[38] Ci WY, Abu Bakar TA, Hamzah E, Saud SN. Study of X-phase formation on Cu-Al-Ni shape memory alloys with Ti addition. JOURNAL OF MECHANICAL ENGINEERING AND SCIENCES 2017;11:27702–2779. https://doi.org/10.15282/jmes.11.2.2017.17.0251.

[39] Mallik US, Sampath V. Influence of quaternary alloying additions on transformation temperatures and shape memory properties of Cu–Al–Mn shape memory alloy. J Alloys Compd 2009;469:156–63. https://doi.org/10.1016/j.jallcom.2008.01.128.

[40] Pinto RDA, Silva RAG. Mirrored symbols, opposite effects: Impact of Ga and Ag additions on the martensite decomposition of the Cu81Al19 alloy. Mater Today Commun 2023;37:107280. https://doi.org/10.1016/j.mtcomm.2023.107280.

[41] Aldirmaz E, Güler · M, Güler · E. Effect of Quaternary Element (Ni and Mn) Additions on Structural and Magnetic Properties of Cu-Based Alloys. Brazilian Journal of Physics 2021;51:1224–9. https://doi.org/10.1007/s13538-021-00926-3.

[42] Zhang X, Liu QS. Influence of alloying element addition on Cu-Al-Ni high-temperature shape memory alloy without second phase formation. Acta Metallurgica Sinica (English Letters) 2016;29:884–8. https://doi.org/10.1007/s40195-016-0467-1.

[43] Karthick S, Shalini S, Mani Prabu SS, Suhel K, Vandan A, Puneet C, et al. Influence of quaternary alloying addition on transformation temperatures and shape memory properties of Cu–Al–Mn shape memory alloy coated optical fiber. Measurement (Lond) 2020;153. https://doi.org/10.1016/j.measurement.2019.107379.

[44] Saud SN, Hamzah E, Abubakar T, Bakhsheshi-Rad HR, Zamri M, Tanemura M. Effects of Mn Additions on the Structure, Mechanical Properties, and Corrosion Behavior of Cu-Al-Ni Shape Memory Alloys. J Mater Eng Perform 2014;23:3620–9. https://doi.org/10.1007/s11665-014-1134-1.

[45] da M. Candido GV, de A. Melo TA, De Albuquerque VHC, Gomes RM, de Lima SJG, Tavares JMRS. Characterization of a CuAlBe Alloy with Different Cr Contents. J Mater Eng Perform 2012;21:2398–406. https://doi.org/10.1007/s11665-012-0159-6.

[46] Canbay CA, Karaduman O, Ünlü N, Özkul I. Study on Basic Characteristics of CuAlBe Shape Memory Alloy. Brazilian Journal of Physics 2021;51:13–8. https://doi.org/10.1007/s13538-020-00823-1.

[47] Başbağ G, Karaduman O, Özkul İ, Canbay CA, Boyrazlı M. Thermo-structural Shape Memory Effect Characterization of Novel CuAlCoMg HTSMA with Ternary Co and Quaternary Mg Addititions. Journal of Materials and Electronic Devices 2022;2:34–9.

[48] Canbay CA, Karaduman O, Özkul İ, Ünlü N. Modifying Thermal and Structural Characteristics of CuAlFeMn Shape Memory Alloy and a Hypothetical Analysis to Optimize Surface-Diffusion Annealing Temperature. J Mater Eng Perform 2020;29:7993–8005. https://doi.org/10.1007/s11665-020-05241-7.

[49] Zare M, Ketabchi M. Effect of chromium element on transformation, mechanical and corrosion behavior of thermomechanically induced Cu–Al–Ni shape-memory alloys. J Therm Anal Calorim 2017;127:2113–23. https://doi.org/10.1007/s10973-016-5839-2.

[50] Karaduman O, Özkul I, Altın S, Altın E, Bağlayan, Canbay CA. New Cu-Al based quaternary and quinary high temperature shape memory alloy composition systems. AIP Conf Proc, vol. 2042, American Institute of Physics Inc.; 2018. https://doi.org/10.1063/1.5078902.

[51] Karaduman O, Aksu Canbay C. Photo-electrical Characterization of New CuAlNi/n-Si/Al Schottky Photodiode Fabricated by Coating Thin-Film Smart Material. Turkish Journal of Science and Technology 2022. https://doi.org/10.55525/tjst.1108761.

[52] Karaduman O, Canbay CA. Investigation of CuAlNi Shape Memory Alloy Doped with Graphene. Journal of Materials and Electronic Devices 2021;3:8–14.
[53] Zhang X, Liu Q. Cu-Al-Ni-V high-temperature shape memory alloys. Intermetallics (Barking) 2018;92:108–12. https://doi.org/10.1016/j.intermet.2017.10.001.
[54] Kissinger HE. Reaction Kinetics in Differential Thermal Analysis. Anal Chem 1957;29:1702–6. https://doi.org/10.1021/ac60131a045.
[55] Chentouf SM, Bouabdallah M, Gachon JC, Patoor E, Sari A. Microstructural and thermodynamic study of hypoeutectoidal Cu-Al-Ni shape memory alloys. J Alloys Compd 2009;470:507–14. https://doi.org/10.1016/j.jallcom.2008.03.009.
[56] Chentouf SM, Bouabdallah M, Gachon J-C, Patoor E, Sari A. Microstructural and thermodynamic study of hypoeutectoidal Cu–Al–Ni shape memory alloys. J Alloys Compd 2009;470. https://doi.org/10.1016/j.jallcom.2008.03.009.
[57] Özkul İ, Karaduman O, Şimşek T, Şimşek T, Canbay CA, Ibrahim PA, et al. Experimental investigation of the effects of different quaternary elements (Ti, V, Nb, Ga, and Hf) on the thermal and magnetic properties of CuAlNi shape memory alloy. J Mater Res 2022;37. https://doi.org/10.1557/s43578-022-00625-y.
[58] Canbay CA, Karaduman O, Ünlü N, Özkul İ. An exploratory research of calorimetric and structural shape memory effect characteristics of Cu–Al–Sn alloy. Physica B Condens Matter 2020;580:411932. https://doi.org/10.1016/j.physb.2019.411932.
[59] Najib ASM, Saud SN, Hamzah E. Corrosion Behavior of Cu–Al–Ni–xCo Shape Memory Alloys Coupled with Low-Carbon Steel for Civil Engineering Applications. J Bio Tribocorros 2019;5. https://doi.org/10.1007/s40735-019-0242-8.
[60] Saud SN, Hamzah E, Abubakar T, Bakhsheshi-Rad HR. Microstructure and corrosion behaviour of Cu-Al-Ni shape memory alloys with Ag nanoparticles. Materials and Corrosion 2015;66:527–34. https://doi.org/10.1002/maco.201407658.
[61] Patterson AL. The Scherrer Formula for I-Ray Particle Size Determination. Physical Review 1939;56:978–82. https://doi.org/10.1103/PhysRev.56.978.